A Study on the Effect of Pulse Electrodeposition Parameters on the Morphology of Pure Tin Coatings

ASHUTOSH SHARMA, SUMIT BHATTACHARYA, SIDDHARTHA DAS, and KARABI DAS

Pure Sn coatings are prepared by pulse current (PC) electrodeposition using aqueous acidic sulfate plating bath. The effects of various electroplating parameters such as current density, additive concentration, duty cycle, frequency, pH, bath temperature, and stirring rate (bath rotation) on the evolution of surface morphology of the coatings have been studied. The as-deposited coatings are characterized by scanning electron microscopy (SEM), X-ray diffraction (XRD), and surface profilometry. It is found that the current density, additive concentration, duty cycle, frequency, and pH have a major influence while temperature and stirring rate of the bath have a minor effect on the grain-size distribution. The mechanism involved in the morphology evolution and grain-size distribution due to the varying electroplating parameters has also been discussed.

DOI: 10.1007/s11661-014-2389-8

I. INTRODUCTION

MICROELECTRONIC components made of Cu and Cu alloys are electroplated with Sn in order to maintain their solderability. However, pure Sn platings are prone to the formation of whiskers which are approximately 1 μm in thickness, and up to several millimeters in length. Their spontaneous formation on microelectronic components can cause short-circuiting, and thus studies based on their mitigation have been conducted since 1950s.[1,2] In the past, lead has been used as an alloying element for tin plating for controlling whisker growth. However, recent environmental regulations, *e.g.*, the European Union's Restriction of Hazardous Substances (RoHS) act have called for the restriction of hazardous substances from electrical and electronic components. RoHS directive is adopted by European Union in February 2003 which restricts the use of six substances, (1) Lead (Pb), (2) Mercury (Hg), (3) Cadmium (Cd), (4) Hexavalent Chromium (Cr^{+6}), (5) Polybrominated Biphenyls (PBB), and (6) Polybrominated Diphenyl Ethers (PBDE). RoHS act not only contributes to the protection of human health, but also deals with the environmentally sound recovery and disposal of waste electrical and electronic equipment. These concerns create interest in other methods of whisker growth mitigation.[3] Various factors that affect whisker growth are surface morphology and microstructure described by plating thickness, grain shape, size and orientation, addition of alloying elements in the Sn plating, external applied stress, and lastly, composition of the substrate.[1,3–8] The surface morphology of electrodeposited metals and alloys is governed by the various electrochemical processes, such as, diffusion and transport of ionic species from the electrolyte toward the electrode, formation of nuclei and growth of the surface.[9,10] The correlation between these phenomena and the evolution of morphology is therefore important in order to manipulate the film microstructure by varying the pulse electrodeposition parameters. For example, in typical applications, dendritic growth is avoided to obtain dense and compact films[11]; however, it is needed where formation of materials with high surface areas is desired.[12] There are several reports on the effects of pulse parameters such as current density, additives, duty cycle, frequency, and stirring rate of bath,[13–16] however, very limited work has been carried out to study the effect of temperature as well as pH on Sn electroplating from acidic baths. This article documents the effect of plating parameters, *i.e.*, current density, additive concentration, duty cycle, frequency, pH, temperature, and stirring rate on the surface morphology of the plating surface. The present study is conducted using simple aqueous acidic stannous sulfate solution. The acidic plating bath is easy to prepare and control, and therefore, investigating the effect of various plating parameters becomes more feasible. In process control, the information about the grain size of materials is very important. This may be useful to predict and/or control various deposit properties like strength, surface roughness, appearance, deposit stress, *etc.* In order to develop an understanding, the role of the electrodeposition parameters, as a design parameter, on grain structure is investigated.

II. EXPERIMENTAL PROCEDURE

Plates of Cu (99.99 pct pure, Alfa Aesar Inc.), 30 mm × 20 mm × 1 mm, are cut and polished using standard metallographic techniques. Prior to electroplating,

ASHUTOSH SHARMA, Research Scholar, SUMIT BHATTACHARYA, Graduate Student, SIDDHARTHA DAS and KARABI DAS, Professors, are with the Department of Metallurgical and Materials Engineering, Indian Institute of Technology Kharagpur, Kharagpur 721302, India. Contact e-mails: karabi@metal.iitkgp.ernet.in; karabi.kgp@gmail.com

Manuscript submitted December 6, 2012.

Published online: 17 June 2014

the substrates (Cu) are cleaned with 10 pct dilute sulfuric acid solution to remove any surface oxide. Then, the prepared Cu plates are electroplated with Sn using acidic electrolyte of the following composition: tin (II) sulfate 20 g/L and sulfuric acid 200 g/L. Triton X-100, a non-ionic surfactant has been used as an organic additive in the bath, to get a uniform deposit on the substrates.

Pulsed electrodeposition is carried out galvanostatically with a potentiostat/galvanostat (Autolab PGSTAT 302N) which can provide cathodic DC square wave pulses. The potentiodynamic polarization behavior of the cathode is carried out using a scan rate of 0.001 V/s and all potentials are referred to Ag/AgCl (3M KCl) electrode. The electrolyte pH is adjusted to 1.0 by the addition of ammonia solution whenever required. A Sartorius Professional meter PP-50 is used to measure both pH and conductivity. The pulse electrodeposition is carried out in an electrolyte of 500 mL volume at room temperature. The anode and the cathode are kept parallel at a distance of 30 mm during the electroplating. The electrolytic bath is agitated continuously using a magnetic stirrer (Tarson SPINOT) rotating at 300 rpm in order to keep the process of deposition continuous by maintaining the concentration of Sn^{+} ions in the electrolyte. The samples are washed and dried immediately after the experiment to remove the adherent additives and bath solution.

The cathodic current efficiency (CCE pct) is calculated by the following equation:

$$\text{CCE (pct)} = 100 \times \frac{M_a}{M_t}, \qquad [1]$$

where M_a is the actual amount of metal deposited and M_t is the theoretically calculated amount of metal according to Faraday's laws.[17] The current efficiency in plating, in general, depends on a number of key parameters of the electrolyte such as chemical component concentrations, current density, additive, duty cycle, frequency, pH, temperature, stirring rate, *etc*., and it decides the final morphology. The as-deposited samples are characterized by SEM (Carl Ziess supra EVO 40). The surface roughness of the electrodeposits is measured by Veeco Dektak profilometer.

III. RESULTS AND DISCUSSION

The effect of different operating bath parameters on the morphology of the coating is investigated and reported in this section. The current efficiency and solution conductivity of the bath, and the measured thickness and roughness of the deposits obtained with different parameters are presented in Table I.

A. *Effect of Current Density*

Current density (j) is one of the most important parameters in electrodeposition. It controls the nucleation and deposition rate. When the current density is varied, a marked change in the morphology of the deposit is observed. Figure 1 shows the morphology of the electrodeposited Sn coatings in response to the different applied current densities. The following discussion is divided into three sections depending on the observed morphology in response to the variation in the current density.

1. *Current density: 0.083 to 0.3 A/cm²*

Figures 1(a) through (d) show the morphology of the deposits electroplated at current densities, varying from 0.083 to 0.3 A/cm^2. The deposit morphology obtained is uniform, bright, and consists of well-developed equiaxed grains with a gradual refinement in grain size. This result is consistent with the previous findings which report that the nucleation rate increases with the current density resulting in a reduction in grain size.[10] The current efficiency increases from 69.8 to 88.45 pct due to the increase in deposition rate within this current density range investigated here.

2. *Current density: 0.5 to 1.0 A/cm²*

When the current density is increased to 0.5 A/cm^2, the equiaxed morphology of the grains changes to dendritic ones, as shown in Figures 1(e) through (f). This type of variation in morphology in response to the current density is due to the fact that if there is a significant increase in the current density, it increases the nucleation rate and is also associated with a higher rate of hydrogen evolution.[18] At this stage, due to high overpotential, the flow rate of Sn^{2+} ions toward cathode is very high causing heavy diffusion of Sn^{2+} ions than its replenishment from solution. Thus, a gradient is created around solution/cathode interface and the deposition is taking place at certain protrusions/nucleation sites on the cathode haphazardly. This results in the development of an unstable growth front giving dendritic structures in a random orientation. This type of unstable growth has also been observed in copper and zinc electrodeposition.[19,20]

The current efficiency in this current density region is poor as compared to that in the previous region, *i.e*., 0.083 to 0.3 A/cm^2. A decreasing current efficiency means an increase in hydrogen evolution and therefore the concentration of depositing species falls. As a consequence, the solution conductivity drops, as shown in Table I.

3. *Current density: 2.0 to 10.0 A/cm²*

When the current density is raised to even higher values, 2 to 10 A/cm^2, a rice type morphology is observed (Figures 1(g) through (i)). Owing to a higher rate of hydrogen evolution in this region, porosity increases throughout the cathode surface. This in turn results in the development of a non-uniform film which depicts a rice type morphology with embedded pores in between them. The porosity causes a less compact deposit, and it is loosely adherent to the cathode.[21]

The rice type features can be explained by the Watanabe's mechanism of metal ion denuded layer (MIDL) formation.[22] During the initial stages of electrodeposition, the Sn^{2+} ions are uniformly distributed all over the cathode. When a potential is applied, the ions adjacent to the cathode region gain electrons from the cathode and get immediately reduced. This ionic discharge induces the

Table I. Current Efficiency and Solution Conductivity of the Bath, and the Measured Thickness and Roughness of the Deposits Plated with Different Parameters, and Appearance of the Various Tin Deposits

Parameter	Roughness (μm)	Conductivity (mS/cm)	Thickness (μm)	CCE (pct)	Visual Appearance
CD (A/cm^2)					
0.083	2.18	46.2	0.49	69.8	BRIGHT SILVERY WHITE
0.1	2.62	47.0	4.06	75.13	BRIGHT SILVERY WHITE
0.2	2.30	46.5	8.84	85.07	BRIGHT SILVERY WHITE
0.3	2.35	45.9	8.36	88.45	SILVERY WHITE
0.5	3.13	45.3	10.88	65.03	GRAY
1	6.57	44.8	12.82	68.1	GRAY
2	7.51	44.9	13.6	66.3	GRAY
5	9.86	40.8	14.2	62.5	DARK GRAY
10	10.05	31.8	15.6	55.02	DARK GRAY
Additive					
0.05	0.49	46.0	8.03	74.22	BRIGHT SILVERY WHITE
0.1	1.78	47.4	8.62	79.76	BRIGHT SILVERY WHITE
0.2	1.83	48	9.21	85.12	BRIGHT SILVERY WHITE
0.5	2.41	45.2	8.90	82.24	BRIGHT SILVERY WHITE
1	2.65	46.3	8.13	75.13	SILVERY WHITE
Duty cycle					
4	0.938	45.2	3.28	67.42	BRIGHT SILVERY WHITE
10	0.69	45.6	8.85	81.74	BRIGHT SILVERY WHITE
20	1.52	46.9	21.3	88.5	SILVERY WHITE
40	1.68	45.8	36.6	76.24	GRAY
60	3.71	46.1	49.9	69.13	GRAY
DC	3.08	47.0	73.7	66.13	DARK GRAY
Frequency (Hz)					
10	2.81	45.3	10.78	99.63	SILVERY WHITE
50	0.65	47.3	10.65	98.41	SILVERY WHITE
100	0.76	47.1	10.14	93.70	SILVERY WHITE
500	0.46	46.8	7.6	70.2	GRAY
pH					
−0.1	1.43	55.5	7.06	65.27	BRIGHT SILVERY WHITE
0.5	1.36	47.9	8.11	74.88	BRIGHT SILVERY WHITE
1	1.06	43.1	9.36	87.73	SILVERY WHITE
2	1.62	40.8	9.50	86.5	SILVERY WHITE
3	3.52	25.7	5.95	55.1	GRAY
Temperature [K (°C)]					
301 (28)	1.48	46.6	9.4	87	BRIGHT SILVERY WHITE
308 (35)	0.94	49.2	10.18	94	BRIGHT SILVERY WHITE
313 (40)	0.85	64.2	10.9	100.73	WHITE YELLOW
323 (50)	0.73	39.8	9.63	89	WHITE YELLOW
333 (60)	1.46	38.2	6.6	61.04	GRAY
Rotation (rpm)					
0	2.8	52.4	6.11	56.50	BRIGHT SILVERY WHITE
100	2.57	48.9	9.53	88.03	SILVERY WHITE
300	2.11	48.6	11.35	93.2	SILVERY WHITE
500	2.7	48.7	9.12	84.22	GRAY
700	1.08	48.3	6.8	63.50	GRAY

beginning of MIDL formation above the cathode surface. Beyond a certain deposit thickness, the MIDL thickness becomes non-uniform since the metal ion discharge process occurs in a random manner at protrusions. The MIDL mechanism states that the metal ions are supplied preferentially at the cathode: (1) the protrusions, where metal ions are supplied, and (2) the underlying valley regions where metal ions are not supplied. As the thickness increases with current density, the film growth at valley regions occurs by the overflow of atoms from the protruded regions. The population density of these dendrites/protrusions will increase with an increase in the current density, as the local current density at the tip is higher than the rest. The smaller the number of protrusions, the faster will be their growth. Thus, at lower current density (<2 A/cm^2), these protrusions will grow over the surface in a random manner. When the current density increases (*i.e.*, 2 to 10 A/cm^2), the population density of these protrusions will rise and the valley region thickness will also increase simultaneously along with protruded region producing a uniform pyramid network. These pyramids are formed in order to minimize the overall surface energy by exposing the lowest energy planes, *i.e.*, {101} planes.[23] Therefore, these pyramids are supposed to be bound by four equivalent {101} surfaces. Figure 2(a) shows a high-resolution SEM image of Figure 1(i) and a schematic diagram of one of the pyramid is shown in Figure 2(b).

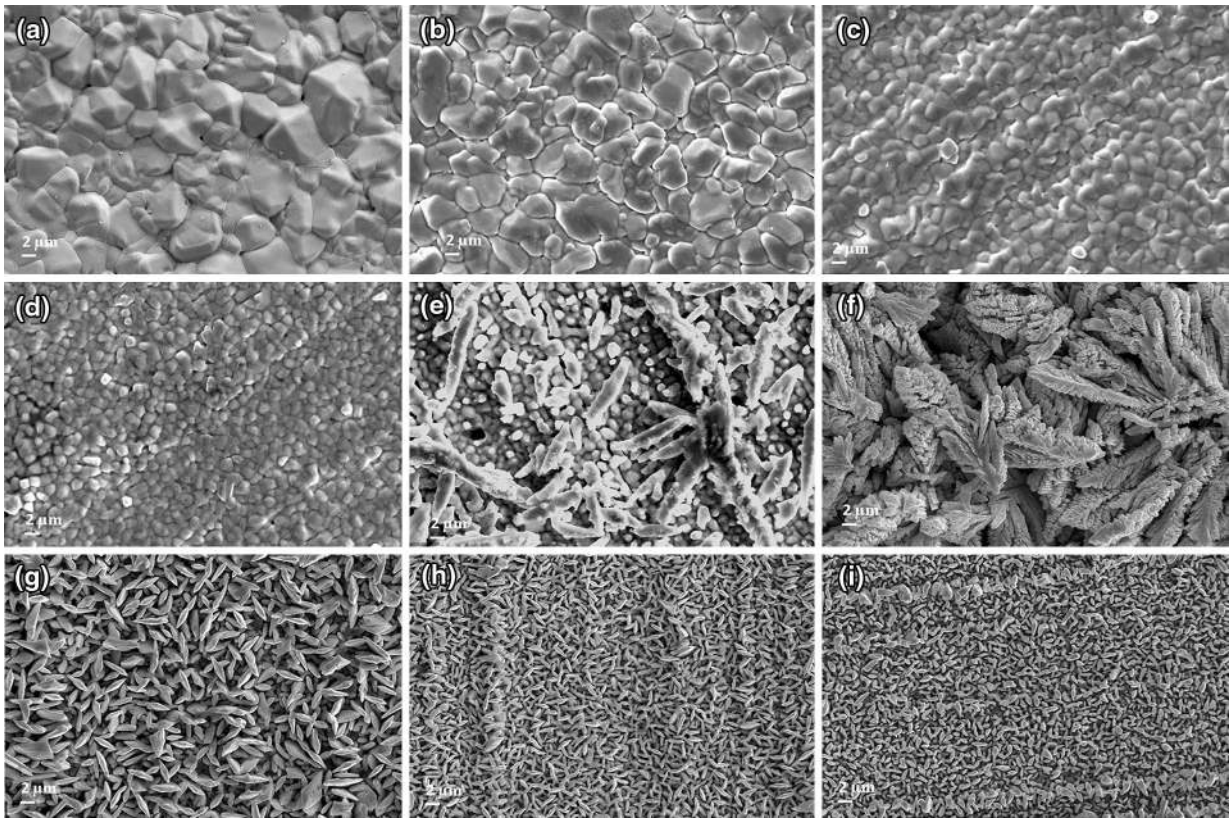

Fig. 1—SEM micrographs showing the morphology of the deposits plated with different current densities (*a*) 0.0833 A/cm^2, (*b*) 0.1 A/cm^2, (*c*) 0.2 A/cm^2, (*d*) 0.3 A/cm^2, (*e*) 0.5 A/cm^2, (*f*) 1.0 A/cm^2, (*g*) 2, (*h*) 5 A/cm^2, and (*i*) 10 A/cm^2.

The rice type network (*i.e.*, consisting of valleys as well as protrusions) in this current density region raises the roughness of the deposits in the range from 7.5 to 10 μm. As compared to the previous regions, the thickness of the deposits increases at a slower rate, due to the decreasing current efficiency. The current efficiency becomes very poor (~55 pct) at 10 A/cm^2, signifying a non-adherent deposit and it can be ascribed to a violent hydrogen evolution. There is also a significant drop in solution conductivity due to the generation of hydrogen gases, especially at 10 A/cm^2.

B. *Effect of Concentration of Additive (Triton X-100)*

It is well known that the additive concentration has a significant effect on the deposition rate and also on the morphology of the deposits. The effect of additive concentration on the cathodic polarization behavior and morphology of the deposit has been studied using Triton X-100 keeping the other bath parameters constant.

1. *Cathodic polarization studies*

A preliminary study of cathodic polarization behavior is carried out in order to understand the deposition mechanism with different additive concentrations. Figure 3 shows the current potential curves recorded at a scan rate of 0.001 V/s, for the Sn plating with different amounts of additive.

It is observed that initially a very small current flows, and nucleation and growth of isolated β-Sn crystals take place at around ~−0.45 V. There is a typical peak as shown in curve a, b, c and d, which indicates the adsorption of Sn atoms on the cathode surface.[24,25] As the current flow increases, the curve enters the corresponding steady regions beyond the peaks, where the reduction of the Sn^{2+} ions to Sn occurs under a steady mass transport control. The deposition mechanism, as proposed by Ichino *et al.*,[26] in this region consists of various redox reactions at the cathode and anode, including the formation of active sites for the Sn deposition and enhancement of the Sn reduction in competition with the hydrogen evolution. The mass transfer region corresponds to the useful region where significant deposition takes place. It is also observed that this steady mass transport region in the curve decreases drastically as the additive concentration increases beyond 0.2 g/L. There is also a substantial shift in the negative potential from −0.45 to −1.2 V as the additive concentration (Triton X-100) increases from 0 to 1 g/L. The negative shift in the reduction potential for tin, in the presence of Triton X-100, is reported to be due to its surface active property, and thus it is expected to be adsorbed at active sites, regions of high local current densities on the electrode surface.[27] This kind of adsorption is potential dependent and there exists an optimum value beyond which the adsorption of Triton

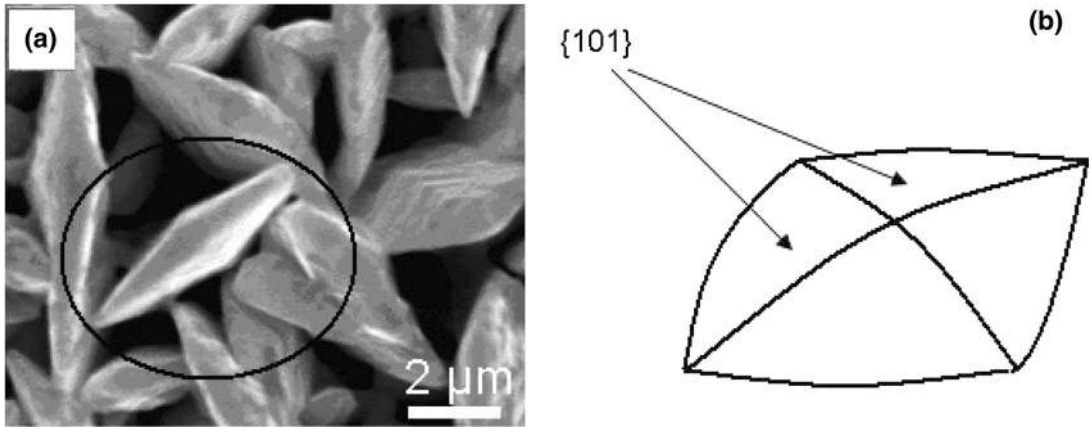

Fig. 2—(*a*) SEM micrograph of the sample deposited at $j = 2$ A/cm^2, encircled within is the morphology of a single pyramid formed, (*b*) schematic of the pyramid formed.

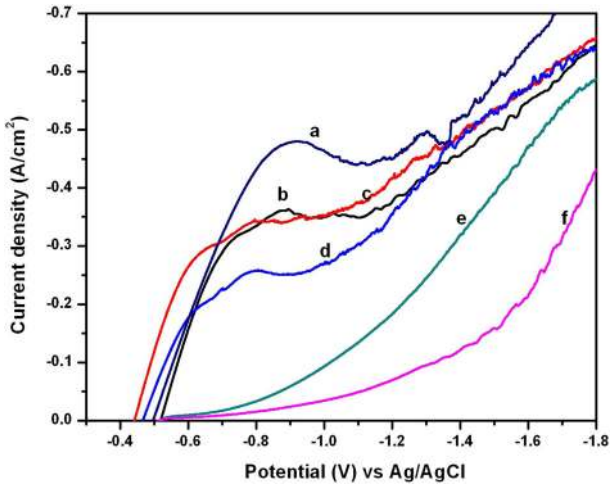

Fig. 3—Cathodic polarization behavior for acidic tin baths with different concentrations of the additive (*a*) 0 g/L, (*b*) 0.05 g/L, (*c*) 0.1 g/L, (*d*) 0.2 g/L, (*e*) 0.5 g/L, and (*f*) 1.0 g/L.

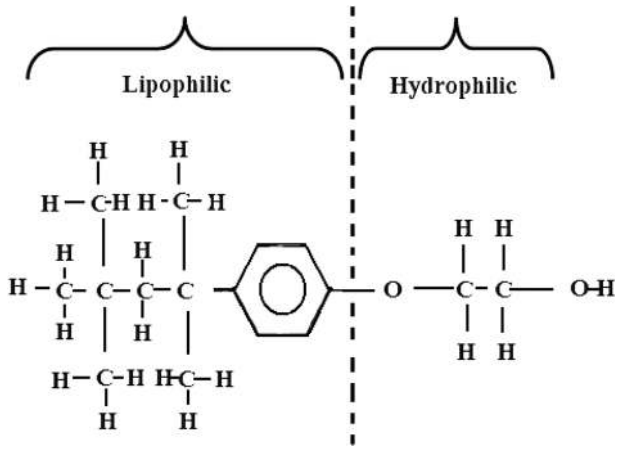

Fig. 4—Chemical structure of Triton X-100.

X-100 on cathode surface decreases. This is confirmed from the observation where with an increase in additive concentration from 0.5 to 1.0 g/L, a drastic shift in negative potential (curve e and f) occurs; this is associated with the desorption of the additive from the cathode surface. This causes an increase in the hydrogen evolution and a lowering in current efficiency from 82.2 to 75 pct, as shown in Table I.

The surface activity of Triton X-100 is due to its interesting chemical structure as shown in Figure 4. It has a hydrophilic polyethylene oxide group and a hydrocarbon lipophilic group.[28] The linking oxygen in oxyethylene chain of this molecule provides a lone-pair of electrons, which interacts with other molecules through hydrogen bonding. This helps in filling in the gaps/pores and thus provides a uniform coating around the cathode.[27,28] In the present case, the negative shifts in reduction potentials and improvement in the bath stability due to Triton X-100 are attributed to such phenomena in the electrolyte.

2. *Surface morphology*

The surface morphology of the developed coatings in response to different amounts of the additive concentration is shown in Figure 5. As discussed already, additives up to a certain concentration are known to have a positive effect on the microstructure of the deposited films in terms of increasing the cathodic polarization.

It is observed from Figure 5(a) that in the absence of an additive the cathode coverage is poor and copper substrate is quite visible, as shown in encircled regions. From Figures 5(b) through (d), a sequential development of equiaxed grain structure is resulting in a slight variation in the deposit roughness, as inferred from Table I. It is also observed that grain structure is deviated from its equiaxed nature when the additive concentration is 0.5 g/L, Figure 5(e) and it becomes more irregular at 1 g/L, Figure 5(f). Therefore, it can be inferred that the additive has a beneficial effect on the morphology up to a certain concentration (*i.e.*, 0.2 g/L). It has been discussed in the previous section that at higher concentration (>0.2 g/L), the cathodic polarization increases (curve e and f). This is associated with progressive evolution of hydrogen gas (caused by the

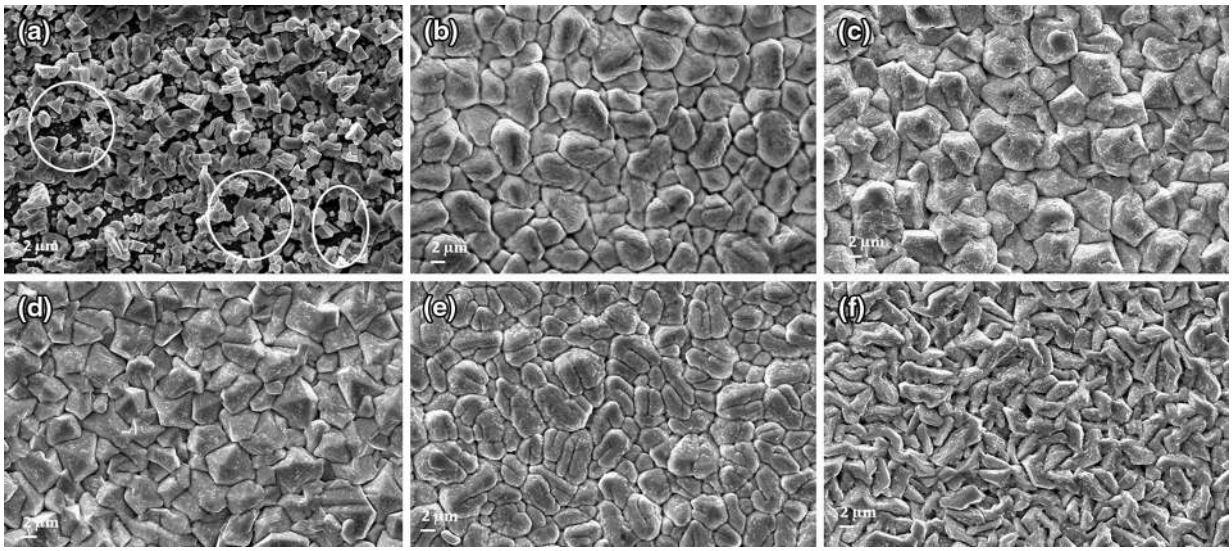

Fig. 5—SEM micrographs showing different morphology evolved due to different concentrations of the additive (*a*) 0 g/L, (*b*) 0.05 g/L, (*c*) 0.1 g/L, (*d*) 0.2 g/L, (*e*) 0.5 g/L, and (*f*) 1.0 g/L. The electrodeposition current density is fixed at 0.2 A/cm^2.

desorption of additive from cathode) leading to the development of non-uniform powdery deposits which is depicted in the corresponding microstructures, Figures 5(e) through (f). The powdery deposits may arise due to the absorption phenomena of the evolved hydrogen gases according to the following reactions[28]:

$$H^+ + e^- \rightarrow H_{ads}, \quad [2]$$

$$2H_{ads} \rightarrow H_2, \quad [3]$$

$$H_{ads} \rightarrow H_{abs}. \quad [4]$$

The additive is expected to block the association of generated hydrogen atoms through Eq. [3]. Thus, the concentration of H_{ads} increases following Eq. [2]. These adsorbed hydrogen atoms get absorbed in the deposits following Eq. [4]. Thus, powdery deposits are obtained. Consequently, the current efficiency decreases and the surface roughness jumps to a higher value, as seen in Table I. A drop in bath conductivity is also noticed beyond 0.2 g/L concentration of Triton X-100. It is observed that at 0.2 g/L concentration of additive, bath conductivity is maximum (48 mS/cm), after which conductivity decreases. This can be owing to the fact that this concentration is very near to the critical micelle concentration where aggregate of surfactant molecules forms (*i.e.*, CMC ~2.4 mM (~0.2 g/L) for Triton X-100). Above this concentration, the micelle formation takes place on the cathode surface, thus blocking the deposition and increasing hydrogen evolution. Therefore, beyond this concentration, the surface morphology turns very rough.[29,30]

C. *Effect of Duty Cycle*

The effect of duty cycle on the morphology of the deposits has been investigated while keeping the peak current density constant at 0.2 A/cm^2 and other parameters constant. The deposition rate in the pulse technique is governed by the PC density (J_p), on time (T_{on}), and off time (T_{off}). At a given peak current density J_p, the duty cycle is given by

$$\text{Duty cycle (Pct)} = \frac{T_{on}}{T_{on} + T_{off}}. \quad [5]$$

Thus, the average current density (J_a) in a pulse electrodeposition is given by

$$J_a = \text{Duty cycle} \times J_p, \quad [6]$$

where J_p is the peak current density.

In the present investigation, duty cycle has been changed by varying the on time while keeping the off time constant. A 100 pct duty cycle means there is no pulse used. The duty cycle combinations are shown in Table II, and the current efficiency, thickness, and roughness values are presented in Table I.

The SEM micrographs of the deposits with different duty cycles are given in Figure 6. The microstructure of the electrodeposit shows a tendency to be finer as the duty cycle and/or T_{on} increase, as shown in Figures 6(a) through (e). Thus, it is concluded that the grain size of the deposits decreases continuously with the increasing

Table II. Pulse Parameters Used for the Deposition of Sn Coatings at Various Duty Cycles

Duty Cycle (Pct)	T_{on} (s)	T_{off} (s)
4	0.00042	0.01
10	0.0011	0.01
20	0.0025	0.01
40	0.0067	0.01
60	0.0150	0.01

on time (at constant T_{off} and J_p) caused by higher overpotentials at a longer current on times. However, at a duty cycle of 100 pct, the grain size observed is much coarser, (Figure 6(f)). Youssef *et al.*[31] have also found the similar behavior for zinc deposits. It is reported that grain size decreases up to 44 pct duty cycle; however, the grain size increases after that. As if the pulse electrodeposition is approaching toward the direct current electrodeposition.[31]

It is also observed from Figure 6 that the deposits are more uniform and less porous in case of the application of PC with lower duty cycles (<20 pct) as compared to that of higher duty cycles (>20 pct). In case of higher duty cycles (>20 pct) and DC current, the porosity increase is due to the increase in average current flow time T_{on}, resulting in an increase in the amount of evolved hydrogen gases. Thus, the surface morphology is very porous and rough. This type of surface morphology can be explained in terms of the dissolved hydrogen and oxygen gases in the electrolyte. The solubility of hydrogen and oxygen in water at 298 K (25 °C) and 1 bar is 1617 and 43.3 mg/L, respectively.[32] Therefore, evolved hydrogen gas is more likely to get dissolved or trapped at the cathode surface as compared to oxygen released from the anode causing inhomogeneous/rough deposits.

The observed minimization of porosity in the case of PC electrodeposition can be attributed to the following factors: (1) the hydrogen and oxygen gas evolved at the cathode may get partly diffused away from the substrate during off time, T_{off} and get suppressed from being incorporated in the deposit during pulse electro-deposition. (2) The discrete amount of gas generated by electrolysis of water during each on time, T_{on} is expected to be significantly less compared to a single continuous DC.[32] The gas evolution and dissipation in the case of PC electrolysis is a dynamic process and it may lead to the formation of micro- to nano-sized bubbles at different sites for each T_{on}. Incorporation of such small bubbles will not produce any big ones in the deposit. Thus, lower duty cycle (<20 pct in our case) results in a smooth morphology as compared to higher ones. The current efficiency increases up to 20 pct duty cycle and then it decreases with further increase in the duty cycle. At higher duty cycles (>20 pct), the hydrogen evolution increases and as a consequence a decrease in current efficiency is observed, as shown in Table I. The roughness is observed to be maximum (~3.08 μm) in case of 100 pct duty cycle.

D. *Effect of Frequency*

The morphology of an electrodeposit is also affected by the frequency of the pulse waveform. The pulse frequency parameters used in the present investigation are shown in Table III.

Frequency of the pulse is described as follows:

$$\text{Frequency}, f(\text{Hz}) = \frac{1}{(T_{on} + T_{off})}. \qquad [7]$$

The morphology variation as a function of frequency is shown in Figures 7(a) through (d). It is observed that at lower pulse frequency (10 Hz), large non-uniform grains of tin have grown with porosity at their boundary edges. With increasing frequency slowly the uniform grains start to develop in a very good morphology at 500 Hz. A lower pulse frequency (f) means a longer pulse cycle ($T = T_{on} + T_{off}$) when the duty cycle is kept constant, Eq. [7]. Thus, at lower pulse frequencies, the pulse duration is higher. This means that more time is available for the charging and discharging of the double layer during T_{on} and T_{off}, respectively. Therefore, the Sn atoms can migrate to the most stable

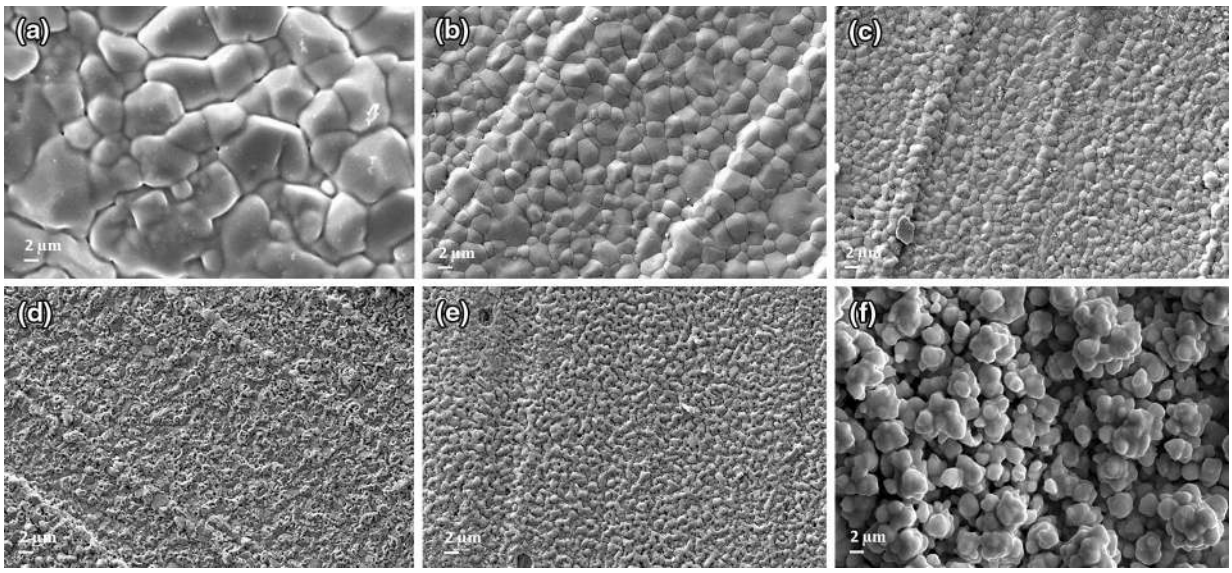

Fig. 6—SEM micrographs showing different morphology evolved due to different duty cycles. (*a*) 4 pct, (*b*) 10 pct, (*c*) 20 pct, (*d*) 40 pct, (*e*) 60 pct, and (*f*) 100 pct (DC). The electrodeposition current density is fixed at 0.2 A/cm^2.

Table III. Pulse Frequency Parameters

10 Hz		50 Hz		100 Hz		500 Hz	
T_{on} (s)	T_{off} (s)	T_{on} (s)	T_{off} (s)	T_{on} (s)	T_{off} (s)	T_{on} (s)	T_{off} (s)
0.01	0.09	0.002	0.018	0.001	0.009	0.0002	0.0018

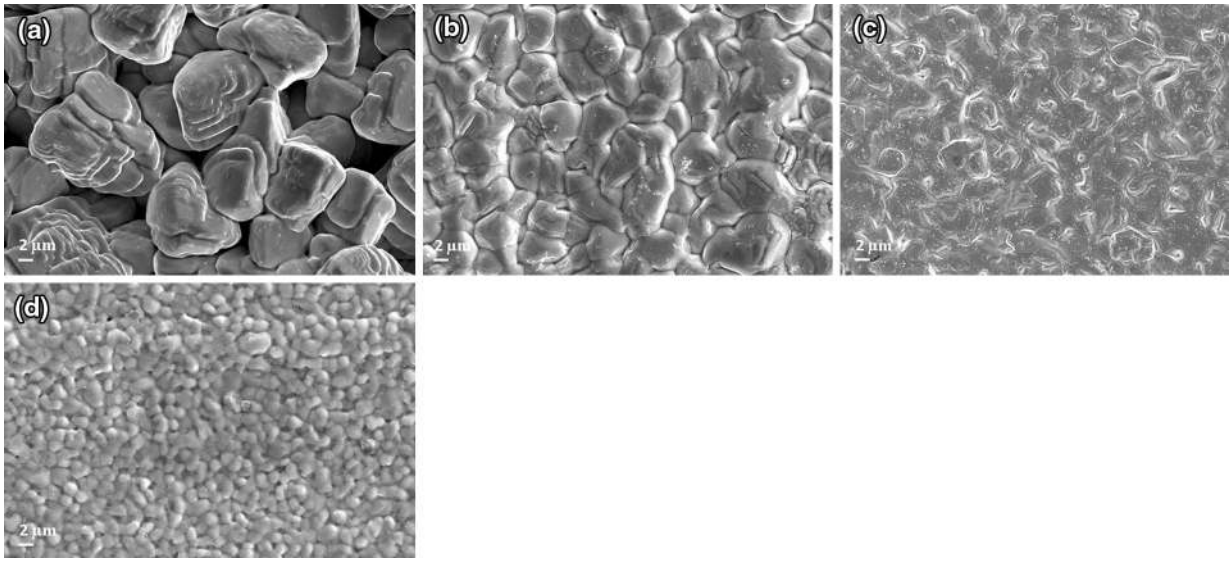

Fig. 7—SEM micrographs showing different morphology evolved due to different frequencies (*a*) 10 Hz, (*b*) 50 Hz, (*c*) 100 Hz, and (*d*) 500 Hz. The electrodeposition current density is fixed at 0.2 A/cm^2.

position and grain growth is favorable. As the pulse frequency increases, the pulses are much shorter, *i.e.*, both T_{on} and T_{off} are of short duration as shown in Table III. Shanthi *et al.*[33] have observed grain refinement during pulse plating of silver alloy during short pulses at higher frequencies; at higher pulse frequencies the double layer does not have sufficient time to fully charge during T_{on} and to discharge during T_{off} time. As soon as the one pulse cycle is completed, the next pulse arrives quickly. These phenomena produce very thin pulse diffusion layers which make the transport and diffusion of the migrating Sn ions from the solution to the cathode surface difficult. This leads to the enhanced nucleation rate with a limited growth rate resulting in a dense microstructure. This type of behavior is also reported by Ibl.[34] The average roughness and thickness of Sn films decrease with the increase in frequency as shown in Table I. The smoothest Sn surface with an average roughness of 0.46 μm is achieved at a frequency of 500 Hz. Initially, the deposits are very thick due to the increased grain growth rate. The thickness drops from 10.78 to 7.6 μm as the frequency changes from 10 to 500 Hz. The corresponding current efficiency also decreases from 99.6 to 70.2 pct.

E. *Effect of pH*

1. *Cathodic polarization behavior*

The effect of pH on the morphology of the tin electrodeposits can be explained using cathodic polarization curves. Figure 8 presents the cathodic polarization curves obtained with the plating bath of different pH values. It is observed that the formation of the isolated Sn nuclei takes place at around ~−0.5 V, and the efficiency for metallic deposition is negligible. As the current increases further with the cathodic potential, a typical peak is observed and a steady-state region is reached where the significant deposition takes place. It is also observed that at lower pH values the peak height for curve a and b, (*i.e.*, current density) is higher and the steady-state mass transport region is minimum. This effect can be correlated with the higher consumption of current by discharge of hydrogen ions at lower pH values.[35,36]

As the pH value increases, the peak height decreases and the steady-state region increases. This increasing trend in the mass transport region with pH signifies a more efficient deposition, as shown in curve c where the steady state region is maximum. The similar trends, as seen in Figure 8, are also reported by previous study on pH effects for metal deposition.[37] The mechanism of stannous reduction from sulfate solution for this region is given by Heusler as follows[38]:

$$Sn + H_2O \rightarrow Sn(OH)^-_{ads} + H^+, \quad [8]$$

$$Sn(OH)^-_{ads} \rightarrow Sn(OH)_{ads} + e^-, \quad [9]$$

$$Sn + Sn(OH)_{ads} \rightarrow Sn_2OH, \quad [10]$$

$$Sn_2OH + OH — SnOH^+ + SnOH_{ads} + 2e^-, \quad [11]$$

$$SnOH^+ + H^+ — Sn^{2+} + H_2O. \quad [12]$$

One more noteworthy point is the absence of steady-state region in the polarization curves (curve d and e), which indicates vigorous hydrogen evolution and a reduction in Sn deposition (*i.e.*, a lowering in current efficiency). At a pH value of 3, there are two peaks observed, which indicates the formation of a second compound. The first peak at −0.55 V signifies deposition of Sn ions while the second peak at −0.82 V indicates the precipitation of the insoluble hydroxides ($Sn(OH)_2$ and $Sn(OH)_4$), *i.e.*, the conversion of stannous (Sn^{2+}) to stannic tin (Sn^{4+}), as shown by Eq. [11]. This result is in agreement with that reported by Salles *et al.* for Zn electrodeposition from sulfate solutions.[37]

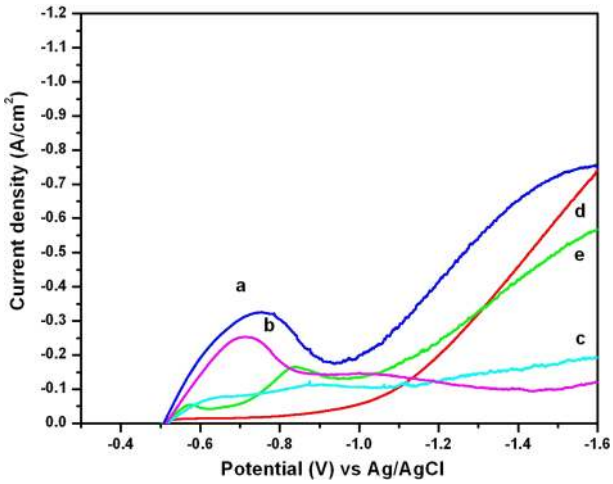

Fig. 8—Cathodic polarization behavior of Sn plating due to different pH (*a*) −0.1, (*b*) 0.5, (*c*) 1.0, (*d*) 2.0, and (*e*) 3.0. The electrodeposition current density is fixed at 0.2 A/cm^2.

2. *Surface morphology*

The morphology of the deposited Sn coatings with different bath pH is shown in Figure 9. It is observed that grain refinement continues to occur as the pH value increases from −0.1 to 1. It can also be confirmed from the polarization behavior of the cathode. At a higher pH of 2 and 3, deposits are more irregular and porous. This can be correlated to hydrogen evolution reaction. At a very high pH 3, powdery deposits are obtained, Figure 9(e). This may be due to the precipitation of stannic hydroxide according to Eq. [11], as described in section III–E–1.

The reason for higher current efficiency when the pH is increased beyond −0.1 to 0.5 is that hydrogen evolution is suppressed with an increase in pH, as shown in polarization curves (b and c). The current efficiency drops to 86.5 to 55 pct from a pH of 2 to 3, and the conductivity of the solution also drops, as shown in Table I.

F. *Effect of Temperature*

Figure 10 shows the morphology of tin deposited at different bath temperatures. All the deposits have been deposited using the constant current density (0.2 A/cm^2), duty cycle (10 pct) and other parameters so that the effect of temperature on the morphology can be analyzed. It is observed from Figure 10(a) that the grains are finer when deposited at room temperature

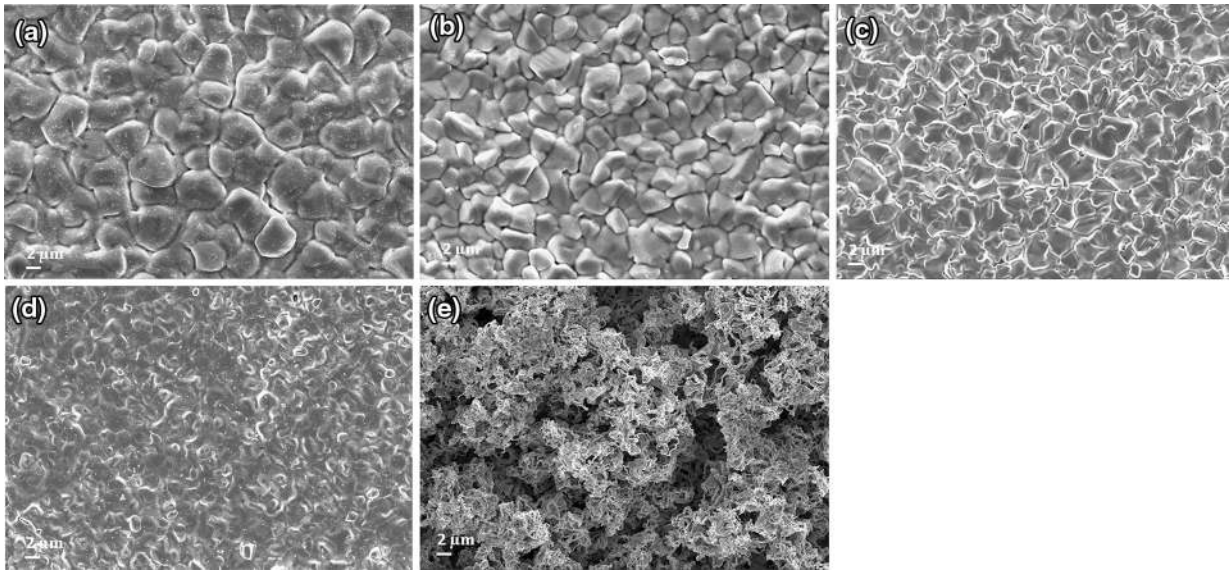

Fig. 9—SEM micrographs showing different morphology evolved due to different pH (*a*) −0.1, (*b*) 0.5, (*c*) 1.0, (*d*) 2.0, and (*e*) 3.0. The electrodeposition current density is fixed at 0.2 A/cm^2.

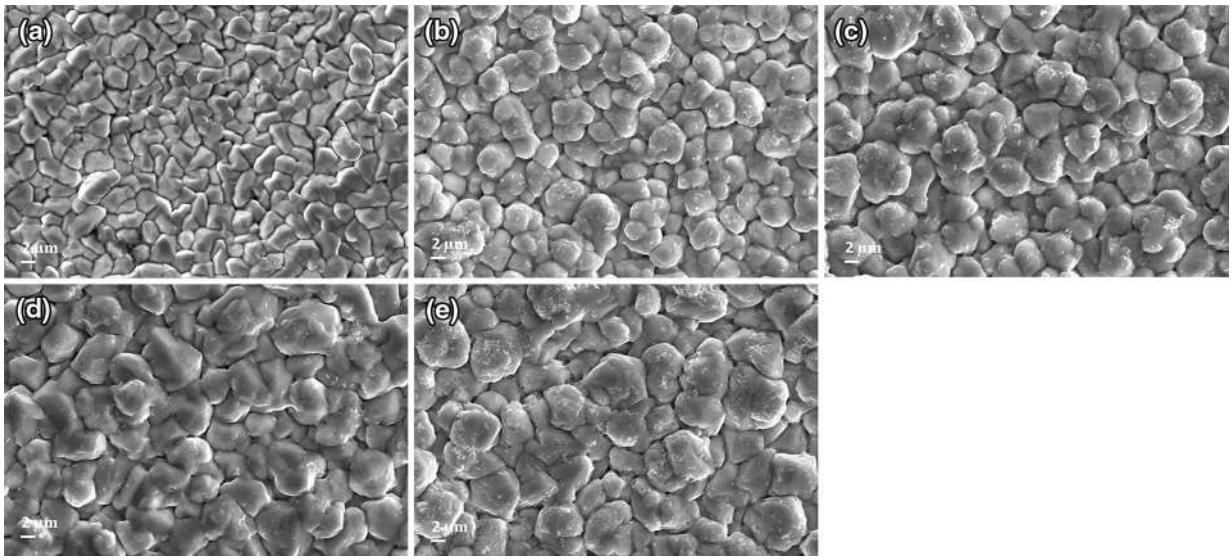

Fig. 10—SEM micrographs showing different morphology evolved due to different bath temperatures kept while deposition (*a*) 301 K (28 °C), (*b*) 308 K (35 °C), (*c*) 313 K (40 °C), (*d*) 323 K (50 °C), and (*e*) 333 K (60 °C). The electrodeposition current density is fixed at 0.2 A/cm^2.

and with a rise in the temperature, it increases, Figures 10(b) through (e). At a high temperature, the mobility of metal ions and inhibiting species increases. Therefore, a higher supply of metal ions toward the cathode decreases the cathodic overpotential.[39] This increases the energy barrier, ΔG, for nucleation process according to the Glasstone equation as referred by Natter *et al.*[39] resulting in coarser grain size at higher temperature:

$$\Delta G \propto \left\{ \frac{1}{\left(\eta + \left[\frac{C'}{C}\right]\right)^2} \right\}, \qquad [13]$$

where C' is the activity of the Sn^{2+} on the electrode and C is the activity of Sn^{2+} in the bulk solution. Moreover, the adsorption rate of inhibitor molecules will decrease at high temperature due to the decrease in viscosity resulting in an increased grain growth.

The current efficiency is maximum at 313 K (40 °C), but then a slight drop is observed. It is reported in the literature that in acidic aqueous solution, the solution may decompose at higher temperature.[40] As a result, the solution bath color turns from light to dark yellow. In the present case, a drop in current efficiency is also noticed above 313 K (40 °C), but there is a little change in morphology of the deposits. A slight decrease in conductivity and thus current efficiency is observed due to the decomposition of chemical species at higher temperatures.

G. *Effect of Stirring Rate (Magnetic Stirring)*

It is interesting to note that the stirring rate of the bath has a very significant effect on the deposit morphology. The deposition parameters except the rpm of the magnetic stirrer which controls the bath agitation are kept constant. The bath agitation has been varied from 0 to 700 rpm.

Figure 11 shows the observed changes in the morphology and grain size with the increase in the stirring rate. It is observed from Figure 11 that during still deposition, the cathode coverage is poor and irregular and non-uniform deposits are obtained. This can be explained as when no rotation is provided, the depositing ions come from the solution and get deposited preferentially on the substrate. Thus, a concentration gradient near the solution/cathode interface is developed. If the gradient becomes too high, the potential required for the deposition goes up and hence the deposition rate goes down significantly. Therefore, initially when no rotation is imparted in bath, the deposition is uneven giving rise to a very poor morphology, Figure 11(a).

As the stirring rate is increased slowly from 50 to 300 rpm, the concentration of ions while coming out from the anode starts to get distributed evenly in the electrolyte. This results in a uniform deposition on the cathodic surface, (Figures 11(b) through (e)). When the stirring rate is increased, the concentration gradient breaks down or is minimized and hence both deposition rate and morphology improve up to 300 rpm. The grain size also increases as a consequence.[41] Further increase in the stirring rate (400 to 700 rpm) causes the ions to reach the electrode surface at a faster speed and decreases the mass transport influence in the process.[42] Whatever ions from solution coming toward the cathode may come for a short span of time and easily fly away due to the turbulent flow of electrolyte. Thus, the deposition rate falls accordingly. This is confirmed from Table I, which shows that the current efficiency is optimum at 300 rpm (93.2 pct). It drops to 63.5 pct at 700 rpm. At a stirring rate of more than 300 rpm, an increase in grain size occurs. This can be related to the Triton X-100 adsorption on the cathode surface which may get disrupted when the flow is turbulent.

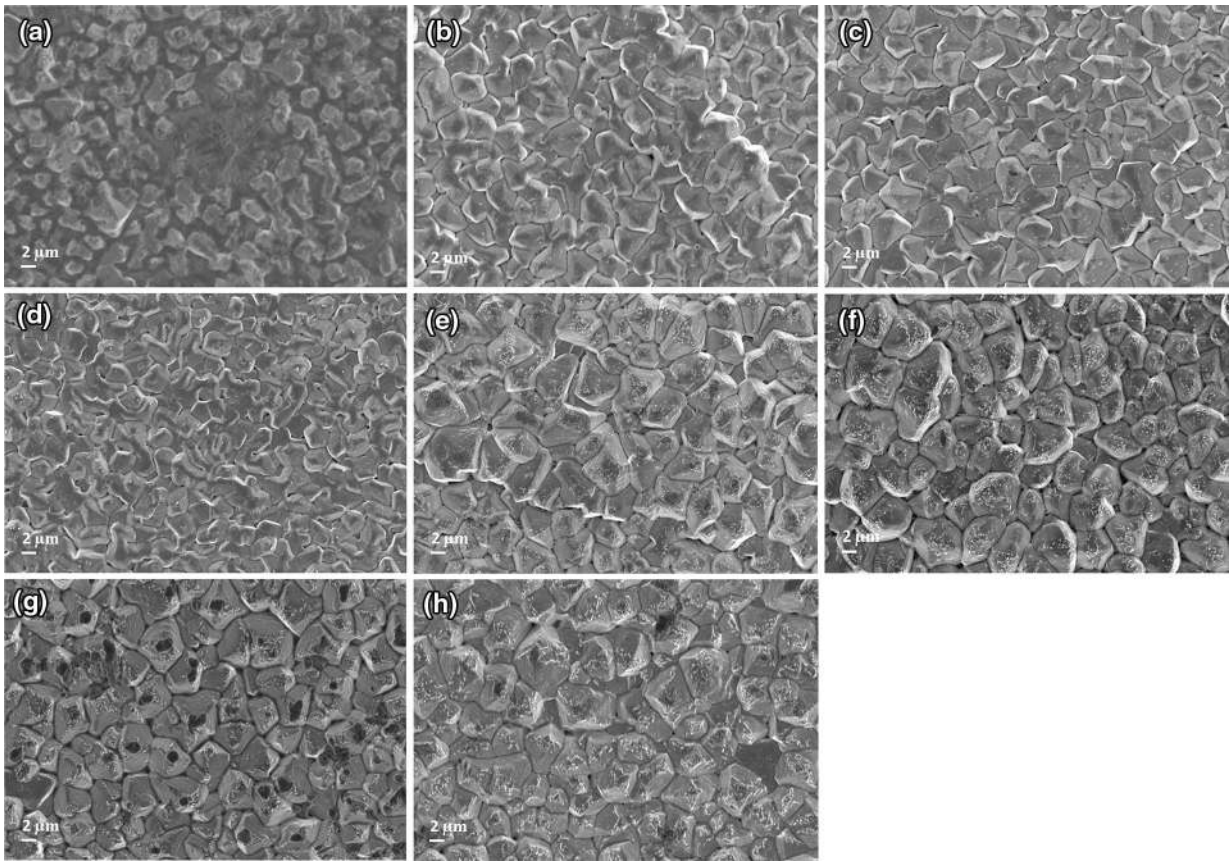

Fig. 11—Different morphology evolved due to different rotation speeds (*a*) 0 rpm, (*b*) 50 rpm, (*c*) 100 rpm, (*d*) 200 rpm, (*e*) 300 rpm, (*f*) 400 rpm, (*g*) 500 rpm, and (*h*) 700 rpm. The electrodeposition current density is fixed at 0.2 A/cm^2.

Furthermore, agitation decreases the deposit roughness to a certain extent.

It can be inferred from the above discussion that the pulse deposition enables the use of high peak current density and overpotential in short periods of pulse on-time, increasing the nucleation rate and improving the deposit morphology. It is shown that to attain the finest possible grain size and smooth deposits, one may choose small duty cycles and high frequencies. It is also possible to increase the deposition current density to a useful range at fixed duty cycle and frequency. Pulse deposition, however, does not improve the morphology in case of high concentration of additive in bath or at very high bath pH. Agitation and temperature are playing a minor role in controlling the grain morphology, however, they have an important role in producing uniform cathode coverage and deposition rate.

IV. SENSITIVITY OF THE VARIABLES

Figure 12 shows the grain-size distribution of the tin coatings in response to the electrodeposition parameters. An increase in current density, additive concentration, pH, duty cycle, and frequency always try to refine the grain size, whereas an increase in temperature and rotation speed increases the grain size. Therefore, an optimum set of parameters should be used to obtain the desired morphology and grain size. A unique morphology of the deposits may be described as having a set of least number of surface perturbations, *i.e.*, protrusions, or outgrowths with well-defined uniform grains. The unusual protruded outgrowths are believed to generate whiskers in long term which is strictly undesirable for a perfect tin surface morphology. In general, such deposits are smooth and exhibit high reflectivity, and tend to have good physical properties as well. This is partially due to low porosity (providing good corrosion and wear resistance) and uniform grain morphology. Therefore, in most of the electroplating applications (decorative or engineering) the aim is to obtain a fine grain, smooth deposit. It is also a noteworthy point that the current efficiency, which controls the deposit thickness and deposition rate of the cathodic deposition, should be high. A solution with a high CCE is always desirable because it tends to deposit on the valleys rather than on the peaks of the growing morphology, resulting in a smooth deposit. However, this may not be always true, *e.g.*, at a frequency of 10 Hz, deposit morphology is poor but CCE is 99.63 pct. The deposit so produced has poor appearance and properties. An increase in CCE is desirable but not at the expense of deposit properties. Therefore, to obtain a desired surface morphology CCE needs to be in proper range as well.

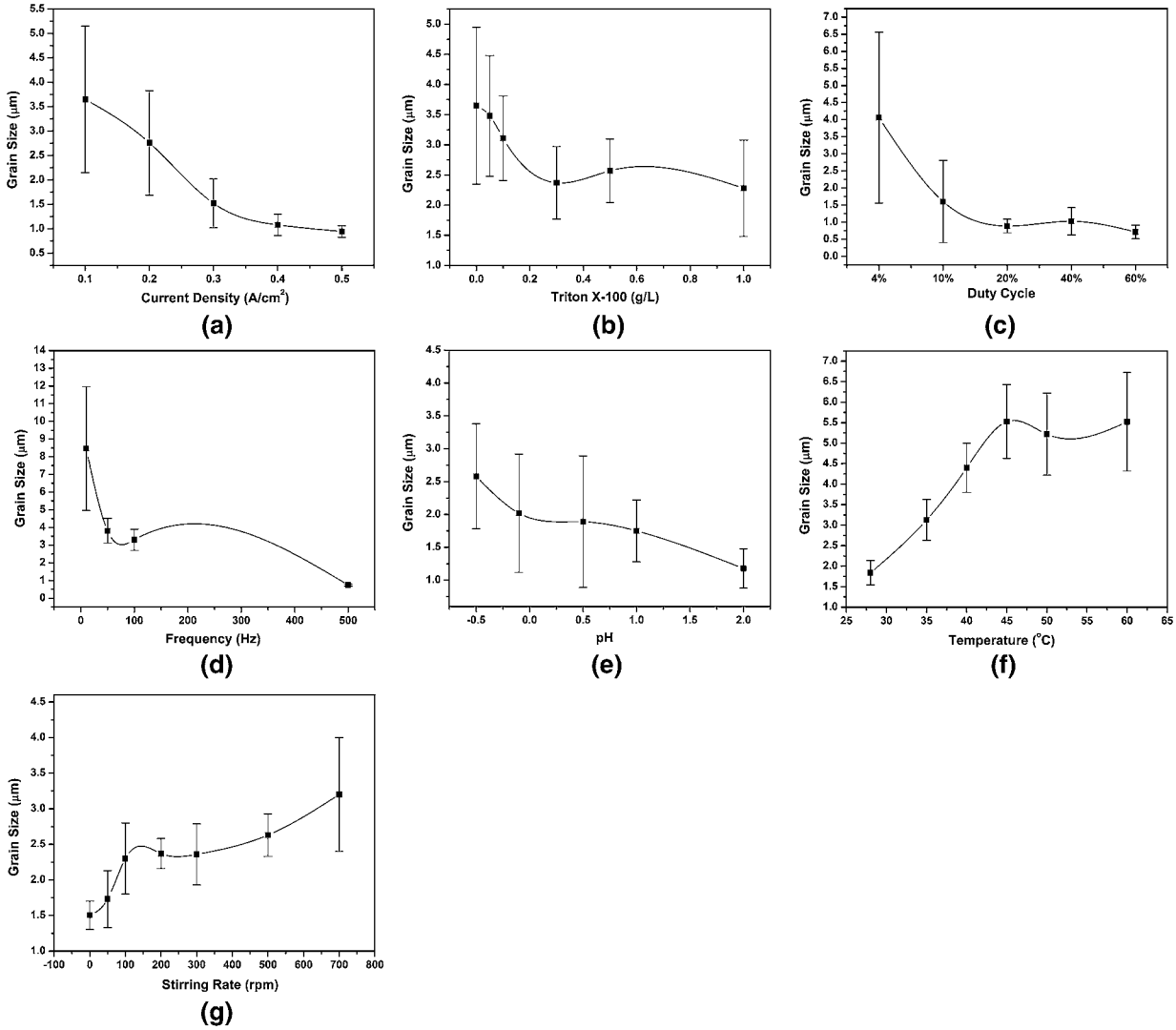

Fig. 12—The grain-size distribution evolved due to different electrodeposition parameters investigated (*a*) current density, (*b*) additive concentration, (*c*) duty cycle, (*d*) pulse frequency, (*e*) bath pH, (*f*) bath temperature, and (*g*) stirring rate.

Temperature and agitation have a minor influence on deposit grain morphology. However, for temperature, one can choose with full freedom the room temperature to avoid even a minute possibility of decomposition of the plating bath.

The optimized parameters, as obtained in the present investigation are j = 0.2 A/cm^2, Triton X-100 = 0.1 g/L, Duty cycle = 10 pct, frequency = 100 Hz, pH 1, temperature = 301 K (28 °C), and stirring rate = 300 rpm.

V. CONCLUSIONS

1. The pulsed current electrodeposition can be an efficient method for the electrosynthesis of tin deposits. The surface morphology of the deposits depends on the electrodeposition parameters which modify the overpotential, directly or otherwise. The current density or overpotential, which controls film nucleation and growth rate, is found to be the most sensitive of all the investigated parameters which influence the morphology of the deposits drastically. The equiaxed grains which form at low current density (<0.3 A/cm^2) change to dendritic ones at 0.5 to 1 A/cm^2, and to the pyramidal ones at a very high current density (2 to 10 A/cm^2).
2. It is found that by changing the duty cycle, the nucleation rate and growth kinetics can be controlled. PC produces the compact and uniform deposits with duty cycles up to 20 pct, while the porosity rises and the surface becomes rough when the duty cycle exceeds 20 pct.
3. Low pulse frequency results in bigger sized grains around 8 to 12 μm at 10 Hz frequency which decreases to 700 nm at 500 Hz. Thus, we can find a combination of 10 pct duty cycle and 100 Hz frequency which gives optimum morphology and current efficiency for this acidic Sn bath.

4. The additive (Triton X-100) concentration also affects morphology. It mainly improves the cathode surface plated finish and improves microstructure if it is added below its critical micelle concentration (*i.e.*, 0.2 g/L).
5. The current density decreases as pH increases. The grain size is found to decrease from 2560 to 1175 nm by increasing the cathodic polarization as the pH value increases from −0.1 to 2. However, as the pH increases to 3, powdery deposits with irregular grains are developed due to the precipitation of stannic hydroxide.
6. An increase in deposition temperature causes the grain size to increase continuously from 1832 nm (room temperature) to 5530 nm (313 K (40 °C)), as expected. Beyond which there is no increase in grain size, however, the solution conductivity and current efficiency decrease drastically due to the oxidation of Sn ions in solution bath.
7. Agitation of the solution provides fresh solution containing metal ions to cathode and thus increases the deposition rate up to 300 rpm and then decreases due to the turbulent flow of the solution where the metal ions fly away from the electrode. A drastic increase in grain size beyond the stirring rate of 300 rpm is caused by a decrease in cathodic overpotential with rotation.

REFERENCES

1. G.T. Gaylon: *Annoted Tin Whisker Bibliography and Anthology*, NEMI Tin Whisker Modeling Project, pp. 1–64, November 2003.
2. H. Leidecker and J. Brusse: *Tin Whiskers, a History of Documented Electrical System Failures*, A Briefing Prepared for the Space Shuttle Program Office, NASA Goddard Jay Brusse/QSS Group, Inc. April 2006.
3. J.W. Osenbach, J.M. DeLucca, B.D. Potteiger, A. Amin, and F.A. Baiocchi: *J. Mater. Sci.*, 2007, vol. 18, pp. 283–305.
4. K.N. Tu and J.C.M. Li: *Mater. Sci. Eng. A.*, 2005, vol. 409, pp. 131–9.
5. T. Kakeshita, K. Shimizu, R. Kawanaka, and T. Hasegawa: *J. Mater. Sci.*, 1982, vol. 17, pp. 2560–566.
6. Y. Zhang, C. Fan, C. Xu, O. Khaselev, and J.A. Abys: *CircuiTree*, 2004, vol. 7, pp. 70–82.
7. K. Whitlaw, A. Egli, and M. Toben: *Circuit World*, 2004, vol. 30, pp. 20–24.
8. J.A. Brusse, G.J. Ewell, and J.P. Siplon: *Tin Whiskers: Attributes and Mitigation*, 22nd Capacitor and Resistor Technology Symposium 2002, New Orleans, LA, 25–29 March 2002, pp. 67–80.
9. L. Durai, R. Dhanasekaran, and P. Ramasamy: *J. Colloid. Interface Sci.*, 1987, vol. 115, pp. 372–77.
10. E. Budevski, G. Staikov, and W.J. Lorenz: *Electrochim. Acta*, 2000, vol. 45, pp. 2559–74.
11. J. Reid: *Jpn J. Appl. Phys.*, 2001, vol. 40, pp. 2650–57.
12. H.C. Shin and M. Liu: *Adv. Funct. Mater.*, 2005, vol. 15, pp. 582–86.
13. K.-W. Moon, S.-K. Kim, M.E. Williams, W.J. Boettinger, and G.R. Stafford: *J. Appl. Electrochem.*, 2010, vol. 40, pp. 1671–81.
14. R. Sekar, C. Eagammai, and S. Jayakrishnan: *J. Appl. Electrochem.*, 2010, vol. 40, pp. 49–57.
15. A. Vicenzo, S. Bonelli, and P.L. Cavallotti: *Trans. Inst. Met. Finish.*, 2010, vol. 88, pp. 248–55.
16. N.M. Martyak and R. Seefeldt: *Electrochim. Acta*, 2004, vol. 49, pp. 4303–311.
17. M. Paunovic and M. Schlesinger: *Fundamentals of Electrochemical Deposition*, 2nd ed., Wiley Interscience, New York, 2006.
18. N.D. Nikolic, K.I. Popov, Lj.J. Pavlovic, and M.G. Pavlovic: *Surf. Coat. Technol.*, 2006, vol. 201, pp. 560–66.
19. N.D. Nikolic, G. Brankovic, and V.M. Maksimovic: *J. Solid State Electrochem.*, 2012, vol. 16, pp. 321–28.
20. K.I. Popov, D.N. Keca, and M.D. Andjelic: *J. Appl. Electrochem.*, 1978, vol. 9, pp. 19–23.
21. Z. Liu, M. Zheng, R.D. Hilty, and A.C. West: *J. Electrochem. Soc.*, 2010, vol. 157, pp. D411–D416.
22. T. Watanabe: *Nano-plating Microstructure Control Theory of Plated Film and Database of Plated Film Microstructure*, 1st ed., Elsevier, Oxford, 2004.
23. U. Sahaym, S.L. Miller, and M.G. Norton: *Mater. Lett.*, 2010, vol. 64, pp. 1547–550.
24. A. Survila, Z. Mockus, and S. Kanapeckaite: *Electrochim. Acta*, 2000, vol. 46, pp. 571–77.
25. Y. Nakamura, N. Kaneko, and H. Nezu: *J. Appl. Electrochem.*, 1994, vol. 24, pp. 569–74.
26. R. Ichino, C. Cachet, and R. Wiart: *Electrochim. Acta*, 1996, vol. 41, pp. 1031–1039.
27. R. Vittal, H. Gomathi, and K.-J. Kim: *Adv. Colloid Interface Sci.*, 2006, vol. 119, pp. 55–68.
28. K. Mitsuda, H. Kimura, and T. Murahashi: *J. Mater. Sci.*, 1989, vol. 24, pp. 413–19.
29. T.C. Franklin: *Surf. Coat. Technol.*, 1987, vol. 30, pp. 415–28.
30. L. Koshy, A.H. Saiyad, and A.K. Rakshit: *Colloid Polym. Sci.*, 1996, vol. 274, pp. 582–87.
31. Kh.M.S. Youssef, C.C. Koch, and P.S. Fedkiw: *J. Electrochem. Soc.*, 2004, vol. 151, pp. C103–C111.
32. L. Besra, T. Uchikoshi, T.S. Suzuki, and Y. Sakka: *J. Eur. Ceram. Soc.*, 2006, vol. 29, pp. 1837–45.
33. C. Shanthi, S. Barathan, R. Jaiswal, R.M. Arunachalam, and S. Mohan: *Mater. Lett.*, 2008, vol. 62, pp. 4519–21.
34. N. Ibl: *Surf. Technol.*, 1980, vol. 10, pp. 81–104.
35. C. Han, Q. Liu, and D.G. Ivey: *Electrochim. Acta*, 2008, vol. 53, pp. 8332–40.
36. O.E. Kongstein, G.M. Haarberg, and J. Thonstad: *J. Appl. Electrochem.*, 2007, vol. 37, pp. 669–74.
37. R.C.M. Salles, G.C.G. de Oliveirab, S.L. Diaza, O.E. Barcia, and O.R. Mattosa: *Electrochim. Acta*, 2011, vol. 56, pp. 7931–39.
38. R. Tunold and A. Broli: *Corros. Sci.*, 1973, vol. 13, pp. 361–73.
39. H. Natter and R. Hempelmann: *J. Phys. Chem.*, 1996, vol. 100, pp. 19525–532.
40. A.C. Tan: *Tin and Solder Plating in the Semiconductor Industry, A Technical Guide*, 1st ed., Chapman and Hall, Cambridge, 1993.
41. S. Wen and J.A. Szpunar: *Electrochim. Acta*, 2005, vol. 50, pp. 2393–99.
42. A.Y. Musa, Q.J.M. Slaiman, A.A.H. Kadhum, and M.S. Takriff: *Eur. J. Sci. Res.*, 2008, vol. 22, pp. 517–24.